

Title: Evidence for Low-valent Electronic Configurations in Iron–Sulfur Clusters

Authors: Alexandra C. Brown, Niklas B. Thompson, and Daniel L. M. Suess*

Affiliations: Department of Chemistry, Massachusetts Institute of Technology, Cambridge, MA, USA

Contact information: suess@mit.edu

Abstract

Although biological iron-sulfur (Fe–S) clusters perform some of the most difficult redox reactions in Nature, they are thought to be composed exclusively of Fe²⁺ and Fe³⁺ ions, as well as mixed-valent pairs with average oxidation states of Fe^{2.5+}. We herein show that Fe–S clusters formally composed of these valences can access a wider range of electronic configurations—in particular, those featuring low-valent Fe¹⁺ centers. We demonstrate that CO binding to a synthetic [Fe₄S₄]⁰ cluster supported by *N*-heterocyclic carbene ligands induces generation of Fe¹⁺ centers via intracluster electron transfer, wherein a neighboring pair of Fe²⁺ sites reduces the CO-bound site to a low-valent Fe¹⁺ state. Similarly, CO binding to an [Fe₄S₄]⁺ cluster induces electron delocalization with a neighboring Fe site to form a mixed-valent Fe^{1.5+}Fe^{2.5+} pair in which the CO-bound site adopts partial low-valent character. These low-valent configurations engender remarkable C–O bond activation without having to traverse highly negative and physiologically inaccessible Fe²⁺/Fe¹⁺ redox couples.

Main Text

Introduction

First characterized over sixty years ago as electron-transfer mediators,^{1,2} Fe–S cluster proteins are now known to have a wide range of functions.^{3,4} Their diverse reactivity includes carrying out some of the most kinetically challenging multi-electron redox reactions in the biosphere,^{4–6} and such reactivity is enabled by the unique chemical properties of their Fe–S cofactors. Despite their prominence in redox biochemistry and the redox versatility of Fe more generally,^{7–10} biological Fe–S clusters are thought to feature only Fe²⁺ and Fe³⁺ ions (and mixed-valent pairs with average oxidation states of Fe^{2.5+}).^{4,5,11} Indeed, no biological Fe–S cluster has been reduced beyond the all-Fe²⁺ state (Figure 1A), and although synthetic [Fe₄S₄(NO)₄] clusters¹² were initially assumed to feature Fe¹⁺ centers,^{13,14} it has since been shown¹⁵ that the Fe centers in these and related clusters are better described as Fe³⁺ centers bound to ³[NO][–] ligands (see SI for further discussion). Additionally, a few super-reduced synthetic Fe–S clusters/complexes have been reported, including an (Fe¹⁺)₂(μ-S) complex,¹⁶ an Fe₂(μ-S) complex in two charge states featuring low-valent Fe (Fe¹⁺Fe²⁺ and 2Fe¹⁺),¹⁷ and a planar [Fe₄S₃] cluster in two charge states featuring Fe¹⁺.¹⁸ In each example, the state with low-valent Fe was generated on an Fe^{2+/1+} redox couple. However, such couples are not thought to be accessible for biological Fe–S clusters.

That biological Fe–S clusters do not access Fe¹⁺ valences limits the d-electron count of their individual sites to $d \leq 6$, which in turn imposes significant limitations on their coordination chemistry. This is illustrated by considering binding and activation of the archetypal π -acidic ligand, CO, at Fe²⁺ ions in varying coordination geometries (Figure 1B). Low-spin, octahedral Fe²⁺–CO complexes are common and famous for their stability, and trigonal bipyramidal, intermediate-spin Fe²⁺–CO complexes have also been reported.^{19–24} In contrast, high-spin, octahedral Fe²⁺–CO complexes are much rarer, have only been characterized at low temperatures, and show no C–O bond activation.²⁵ These differences in CO activation and binding strength can be rationalized by the occupation of the two Fe–CO π -backbonding orbitals; both

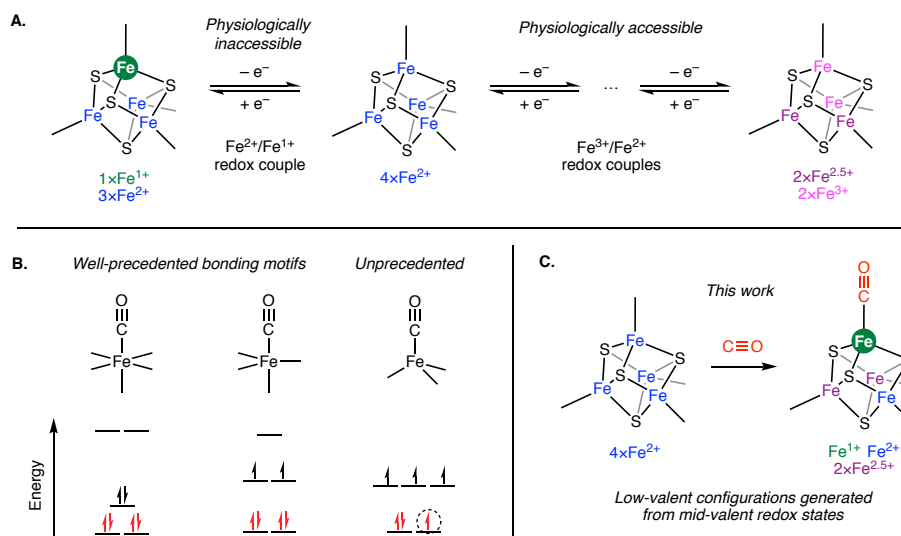


Figure 1. Inability of biological Fe–S clusters to access low-valent states and its consequences for small molecule activation. (A) $[\text{Fe}_4\text{S}_4]$ clusters as a case study: redox chemistry at Fe–S clusters occurs on $\text{Fe}^{3+/2+}$ redox couples with $\text{Fe}^{2+/1+}$ couples being physiologically inaccessible. (B) Basis for weak CO binding and activation at high-spin Fe^{2+} centers: partial occupation of π -backbonding orbitals (circled). (C) This work demonstrates that Fe–S clusters formally comprised of Fe^{2+} and/or Fe^{3+} centers can access low-valent Fe through redox disproportionation, thereby attaining electronic configurations that allow for strong bond activation while avoiding $\text{Fe}^{2+/1+}$ redox couples.

low-spin octahedral and intermediate-spin trigonal bipyramidal geometries allow full occupation of the π -backbonding orbitals, whereas a high-spin configuration results in only partial occupation of these orbitals, leading to diminished CO binding affinity and activation. Consistent with this logic, no tetrahedral CO adduct of Fe^{2+} has been isolated; such a complex would be high-spin with partially unoccupied π -backbonding orbitals, and would therefore have an extremely low affinity for CO.

Given these observations from mononuclear Fe chemistry, it is perhaps surprising that Fe–S clusters featuring high-spin, mid-valent Fe centers (Fe^{2+} and Fe^{3+}) have emerged as promising catalysts for reducing CO and other π -acidic ligands. For example, nitrogenases reductively couple CO to hydrocarbons,^{26–29} and this Fischer-Tropsch-type chemistry has been further demonstrated for a wide range of Fe–S clusters both bound to and isolated from protein hosts.^{30–36} The unusual ability of Fe–S clusters to activate CO stands in contrast to the predicted inability of analogous high-spin, mid-valent

mononuclear Fe complexes to bind CO, let alone to engender strong C–O bond activation. This fundamental disconnection prompted us to examine the geometric and electronic structures of CO-bound Fe–S clusters; below we detail unexpected links between Fe–S clusters and low-valent Fe chemistry and demonstrate that, in fact, Fe–S clusters can access low-valent configurations that give rise to exceptional C–O bond activation.

Results and Discussion

To study CO binding and activation at an Fe–S cluster, we utilized synthetic [Fe₄S₄] clusters in which three Fe centers are each supported by the sterically protective *N*-heterocyclic carbene (NHC) ligand, IMes (1,3-dimesitylimidazol-2-ylidene); this arrangement leaves the remaining Fe site available for substrate binding.³⁷ Our approach to preparing CO-bound clusters was to abstract Cl• or Cl[−] from (IMes)₃Fe₄S₄Cl (**1-Cl**) in the presence of CO. We expected to observe the formation of polycarbonylated clusters featuring low-spin Fe sites^{38,39} and/or bridging CO structures,^{40–42} and we predicted that the simplest structures—those featuring a single CO bound to the unique, tetrahedral Fe site—would be thermodynamically unfavorable for the reason articulated above: [Fe₄S₄]⁺⁰ clusters composed of tetrahedral Fe²⁺ and Fe³⁺ sites should have very weak affinity for CO.

To our surprise, the terminal, monocarbonylated adducts are in fact the products of these reactions. Specifically, reduction of **1-Cl** via Cl• abstraction using Ti(N[^{*t*}Bu]Ar)₃ (Ar = 3,5-dimethylphenyl)⁴³ in the presence of CO generates the cluster (IMes)₃Fe₄S₄CO (**1-CO**) in 78% yield with loss of ClTi(N[^{*t*}Bu]Ar)₃ (Fig. 2A). Cluster **1-CO** has an *S* = 2 ground state as established by EPR spectroscopy and SQUID magnetometry (see SI). The cyclic voltammogram of **1-CO** shows a reversible oxidation event at −1.54 V vs. Fc/Fc⁺ corresponding to the [Fe₄S₄]^{0/1+} couple and an irreversible oxidation at ca. −0.5 V corresponding to oxidation of [**1-CO**]⁺ (see SI). The [Fe₄S₄]^{0/1+} couple is ca. 400 mV more positive than other reported [Fe₄S₄]^{0/+} redox couples^{44–46} owing to the cluster's strongly π-accepting CO ligand. The one-electron oxidized cluster, [(IMes)₃Fe₄S₄CO]⁺ ([**1-CO**]⁺), was prepared from **1-Cl** by Cl[−] abstraction using Na[BArF₄] ([BArF₄][−] = tetrakis[3,5-bis(trifluoromethyl)phenyl]borate) in the presence of CO and has an *S* = 1/2 ground state (see SI). Both complexes were fully characterized and their structures were confirmed by single-crystal X-ray diffraction (Fig. 2B and 2C); we discuss their structural and spectroscopic properties in greater detail below.

A striking property of **1-CO** and [**1-CO**]⁺ is the extent to which their CO ligands are activated. Indeed, their C–O stretching frequencies of 1832 cm^{−1} and 1902 cm^{−1}, respectively, are comparable to

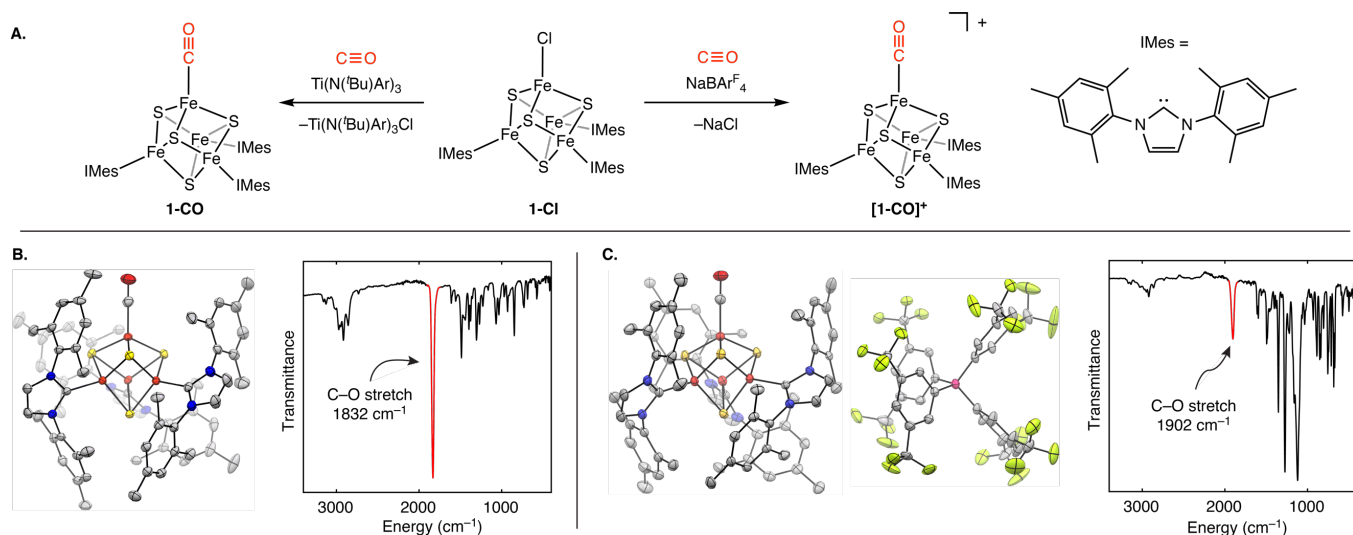


Figure 2. Synthesis and characterization of CO-bound $[\text{Fe}_4\text{S}_4]$ clusters. (A) Synthesis of **1-CO** and **[1-CO]⁺**. Ar = 3,5-dimethylphenyl; Ar^F = 3,5-bis(trifluoromethyl)phenyl. Structural and infrared spectroscopic characterization of (B) **1-CO** and (C) **[1-CO]⁺**. Thermal ellipsoid plots shown at 50% probability with carbon (gray), iron (orange), sulfur (yellow), nitrogen (blue), oxygen (red), boron (pink) and fluorine (green). Solvent molecules and H-atoms are omitted for clarity. The C–O stretches in the IR spectra are highlighted in red.

those of mononuclear $\text{Fe}^{1+}\text{-CO}$ complexes, ($\nu(\text{C-O}) = 1850\text{--}1907\text{ cm}^{-1}$)^{22,23,47} and intermediate spin $\text{Fe}^{2+}\text{-CO}$ complexes ($\nu(\text{C-O}) = 1899\text{--}1966\text{ cm}^{-1}$).^{19–24} Such remarkable degrees of C–O activation for **1-CO** and **[1-CO]⁺** are inconsistent with what would be expected for a high-spin $\text{Fe}^{2+}\text{-CO}$ center, for which $\nu(\text{C-O})$ would be $> 2100\text{ cm}^{-1}$.²⁵

The high degree of C–O activation in **1-CO** and **[1-CO]⁺** necessitates reevaluation of our initial assumptions about their electronic structures, namely that the tetrahedral Fe centers in these clusters are each high-spin, $d^6\text{ Fe}^{2+}$ or $d^5\text{ Fe}^{3+}$. There are two scenarios that would enable full occupation of the Fe–CO π -backbonding orbitals, and thereby account for the observed strong C–O activation: either the Fe–CO site could maintain an Fe^{2+} valence and adopt a low- or intermediate-spin electronic configuration, or it could adopt a low-valent configuration. Although computational analysis can provide insights into the local spin state of the Fe–CO site (*vide infra*), this information is difficult to extract experimentally. Nevertheless, we disfavor the first hypothesis in part because the Fe–CO sites in **1-CO** and **[1-CO]⁺** display nearly perfect tetrahedral geometries ($\tau_4 = 0.92$ in both **1-CO** and **[1-CO]⁺**, where τ_4 is a

parameterization of four-coordinate geometries that takes on a value of 1 for a perfect tetrahedron)⁴⁸ imposed by the cuboidal structure of the cluster. In contrast, four-coordinate intermediate-spin Fe²⁺ complexes exhibit a significant distortion from tetrahedral symmetry.^{49–51} We therefore designed experiments to test the alternative hypothesis that the Fe–CO sites adopt low-valent configurations.

Mössbauer spectroscopy is widely used to determine the valences of Fe sites in Fe–S clusters.^{52,53} In particular, the isomer shift reflects both the formal Fe valence and the covalency of Fe–ligand bonding, where a higher isomer shift corresponds to a lower valence and decreased Fe–ligand covalency. These trends move in concert for typical Fe–S clusters (*i.e.*, those ligated by π -donor ligands such as thiolates), but they counteract one another for Fe sites featuring strong π -acceptors such as CO.⁵⁴ For the latter, a lower valence would engender stronger Fe–CO covalency via π -backbonding, and these two effects would impact the isomer shift in opposing directions. For this reason, the valences of the Fe–CO sites in **1-CO** and [**1-CO**]⁺ cannot be directly inferred from their isomer shifts. We therefore analyzed the valences of the NHC-ligated sites in **1-CO** and [**1-CO**]⁺ and used this information to deduce the valences of the CO-ligated Fe sites.

Determination of the valences of the NHC-ligated sites in **1-CO** and [**1-CO**]⁺ requires suitable reference molecules for which the valences are well-established. For these purposes, we examined the Mössbauer spectroscopic properties of the homoleptic, NHC-ligated clusters, [I^{Pr}Me₄Fe₄S₄]^{0/+} (**2** and [**2**]⁺; I^{Pr}Me = 1,3-diisopropyl-4,5-dimethylimidazol-2-ylidene),^{37,46} which have the same [Fe₄S₄] core electron count as **1-CO** and [**1-CO**]⁺, respectively. The Mössbauer spectrum of **2** in Fig. 3A is consistent with previous reports^{46,55} and features a 3:1 pattern of peaks representing the three coaligned Fe²⁺ centers and the one antiferromagnetically coupled Fe²⁺ center, respectively. The Mössbauer spectrum of [**2**]⁺ has not been previously described; it displays a single quadrupole doublet ($\delta = 0.48 \text{ mm s}^{-1}$ and $|\Delta E_Q| = 1.34 \text{ mm s}^{-1}$; Fig. 3 and Table 1) indicating complete valence averaging for [**2**]⁺ on the Mössbauer timescale. The average isomer shift (δ_{avg}) of the Fe centers in **2** and [**2**]⁺ is 0.60 and 0.48 mm s⁻¹, respectively (80 K, Fig. 3), and the magnitude of the decrease in δ_{avg} upon oxidation (0.12 mm s⁻¹ for a 0.25 electron oxidation per

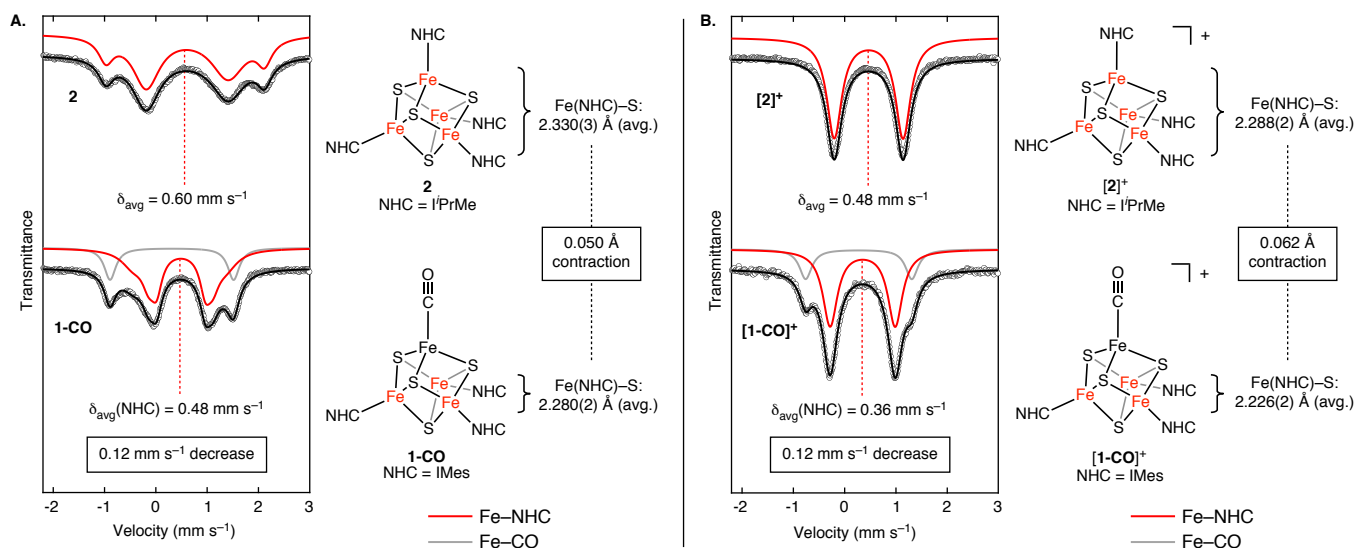


Figure 3. Spectroscopic and structural evidence for low-valent Fe configurations in $[\text{Fe}_4\text{S}_4]\text{-CO}$ complexes. (A) 80 K Mössbauer spectra of **2** (top left) and **1-CO** (bottom left) and contraction of (NHC)Fe–S distances upon CO binding (right). (B) 80 K Mössbauer spectra of $[2]^+$ (top left) and $[1\text{-CO}]^+$ (bottom left) and contraction of (NHC)Fe–S distances upon CO binding (right). Red and gray lines show simulated parameters for the NHC- and CO-ligated Fe centers, respectively. The total simulations are shown in black. See Table 1 for tabulated parameters.

Table 1. Mössbauer and structural parameters for **1-CO**, **2**, $[1\text{-CO}]^+$, and $[2]^+$.^a

	Mössbauer parameters				Structural parameters			
	NHC-bound Fe (avg.)		CO-bound Fe		NHC-bound Fe (avg.)		CO-bound Fe (avg.)	
	δ (mm s ⁻¹)	$ \Delta E_Q $ (mm s ⁻¹)	δ (mm s ⁻¹)	$ \Delta E_Q $ (mm s ⁻¹)	Fe–S (Å)	Fe–C (Å)	Fe–S (Å)	Fe–C (Å)
1-CO	0.48	1.34	0.32	2.408	2.280(2)	2.053(2)	2.259(1)	1.772(2)
2	0.60	1.97	—	—	2.330(3)	2.109(5)	—	—
$[1\text{-CO}]^+$	0.36	1.27	0.28	2.069	2.226(2)	2.029(2)	2.199(1)	1.789(2)
$[2]^+$	0.48	1.34	—	—	2.288(2)	2.060(5)	—	—

^a: The uncertainty in the average of Fe–S and Fe–C bond lengths is given as the root sum of the squares of the individual estimated standard deviations.

Fe site) is similar to what has been observed in other Fe–S clusters.⁵² Note that we and others⁵² prefer to extrapolate valences using δ_{avg} because the isomer shifts of individual sites with the same formal valence can vary depending on the nature of the Fe–Fe coupling^{46,55} and additionally because δ_{avg} does not depend on the model used to fit the quadrupole doublets arising from multiple spectroscopically unique Fe centers.

In the Mössbauer spectra of **1-CO** and [**1-CO**]⁺ (Fig. 3 and Table 1), the quadrupole doublets corresponding to the Fe–CO sites can be readily identified by their low isomer shifts (0.32 mm s⁻¹ in **1-CO** and 0.28 mm s⁻¹ in [**1-CO**]⁺) and large quadrupole splittings (2.408 mm s⁻¹ in **1-CO** and 2.069 mm s⁻¹ in [**1-CO**]⁺). The low isomer shifts for the Fe–CO sites are similar to those observed for low-valent Fe–CO complexes^{22,23} and reflect high Fe–CO covalency as a result of π -backbonding with CO. The large quadrupole splitting is likewise consistent with significant Fe–CO π -backbonding, which increases the anisotropy of the local electric field gradient. The remaining Mössbauer signals arise from the NHC-ligated sites and can be modeled as three quadrupole doublets for **1-CO** (see SI) and a single quadrupole doublet for [**1-CO**]⁺; similarly to [**2**]⁺, the latter exhibits full valence delocalization amongst its NHC-ligated sites on the timescale of the Mössbauer experiment. For both **1-CO** and [**1-CO**]⁺, the δ_{avg} values for the NHC-ligated sites—0.48 mm s⁻¹ and 0.36 mm s⁻¹, respectively—are 0.12 mm s⁻¹ lower than those in their homoleptic congeners, which suggests that the NHC sites in **1-CO** and [**1-CO**]⁺ are significantly more oxidized than the NHC sites in **2** and [**2**]⁺. As deduced from the Mössbauer spectra of **2** and [**2**]⁺ (*vide supra*), the magnitude of this change in the average isomer shift—0.12 mm s⁻¹—corresponds to an oxidation of 0.25 electrons per Fe center, and the average valence of the NHC-ligated Fe sites in **1-CO** and [**1-CO**]⁺ are therefore estimated to be Fe^{2.25+} and Fe^{2.5+}, respectively (compared with Fe²⁺ and Fe^{2.25+} for **2** and [**2**]⁺, respectively). In aggregate, the three NHC-ligated sites in **1-CO** and [**1-CO**]⁺ are 0.75 electrons more oxidized than the analogous Fe–NHC sites in **2** and [**2**]⁺, respectively, leaving the Fe–CO site in each cluster 0.75 electrons more reduced. Thus, based on this analysis, the experimentally deduced Fe–CO valences in **1-CO** and [**1-CO**]⁺ are Fe^{1.25+} and Fe^{1.5+}, respectively.

The structural parameters of **1-CO** and [**1-CO**]⁺ are also consistent with intramolecular charge transfer from the Fe–NHC sites to the Fe–CO sites (Fig. 3 and Table 1). The NHC-bound Fe sites in **1-CO** and [**1-CO**]⁺ display shorter average Fe–S distances (by ~0.05 Å) and Fe–C(NHC) distances (by 0.06 Å for the neutral clusters and 0.031 Å for the cationic clusters) relative to those in **2** and [**2**]⁺. Both trends are expected to follow from enhanced donation from the sulfide and NHC ligands to the NHC-bound Fe

sites in **1-CO** and $[\mathbf{1-CO}]^+$, and are thereby consistent with the conclusions from the Mössbauer spectroscopic analysis: the NHC-bound Fe sites are more oxidized in the CO complexes than in the homoleptic, NHC-bound clusters. Shortened Fe–S bonds were also observed in a recent computational model of a CO-bound nitrogenase intermediate featuring a four-coordinate Fe–CO site.⁵⁶

The experimental picture described above—massive C–O bond activation and charge depletion at the NHC-bound sites—is consistent with substantial charge redistribution among the Fe–NHC and Fe–CO sites, resulting in electronic configurations featuring low-valent, CO-bound Fe centers. We further evaluated the electronic structures of these clusters using broken-symmetry density functional theory calculations (BS-DFT; TPSS and TPSSh functionals and def2-TZVP basis sets), analyzed the BS-DFT solutions in terms of localized molecular orbitals, and demonstrated that the experimental Mössbauer parameters are reproduced *in silico* (see SI). As expected, the computed localized orbitals of **2** and $[\mathbf{2}]^+$ are consistent with the canonical electronic structures of $[\text{Fe}_4\text{S}_4]^0$ and $[\text{Fe}_4\text{S}_4]^+$ clusters (featuring $4\times\text{Fe}^{2+}$ centers for **2** and $2\times\text{Fe}^{2+}$ and $2\times\text{Fe}^{2.5+}$ centers for $[\mathbf{2}]^+$). In contrast, the localized orbital calculations and Löwdin population analyses of **1-CO** indicate that it adopts an unprecedented electronic structure for $[\text{Fe}_4\text{S}_4]^0$ clusters; rather than featuring $4\times\text{Fe}^{2+}$ ions, the Fe valences in **1-CO** consist of $1\times\text{Fe}^{1+}\text{-CO}$, $1\times\text{Fe}^{2+}$, and $2\times\text{Fe}^{2.5+}$ (Fig. 4A). The occupied valence orbitals on the CO-bound Fe include five β -spin and two α -spin orbitals with primarily Fe 3d character, four of which have symmetry that allows for π -backbonding with CO. In **1-CO**, the oxidized counterpart to the one-electron-reduced Fe–CO site is a mixed-valent pair of $2\times\text{Fe}^{2.5+}$ ions in which the hole is delocalized over two Fe centers via the double-exchange mechanism (Fig. 4A).⁵⁷ In addition, the Fe^{2+} site adopts a local $S = 1$ configuration; such non-Hund configurations have been observed in BS-DFT calculations of other Fe–S clusters.^{58,59}

The BS-DFT calculations on $[\mathbf{1-CO}]^+$ are complicated by a dependence of the calculated electronic structure on the functional (see SI). Calculations using the TPSS functional arrive at an electronic structure in which the two π -backbonding orbitals on the Fe–CO site are fully occupied and localized on the Fe–CO site, and one of the unpaired electrons on this site is delocalized onto a spin-

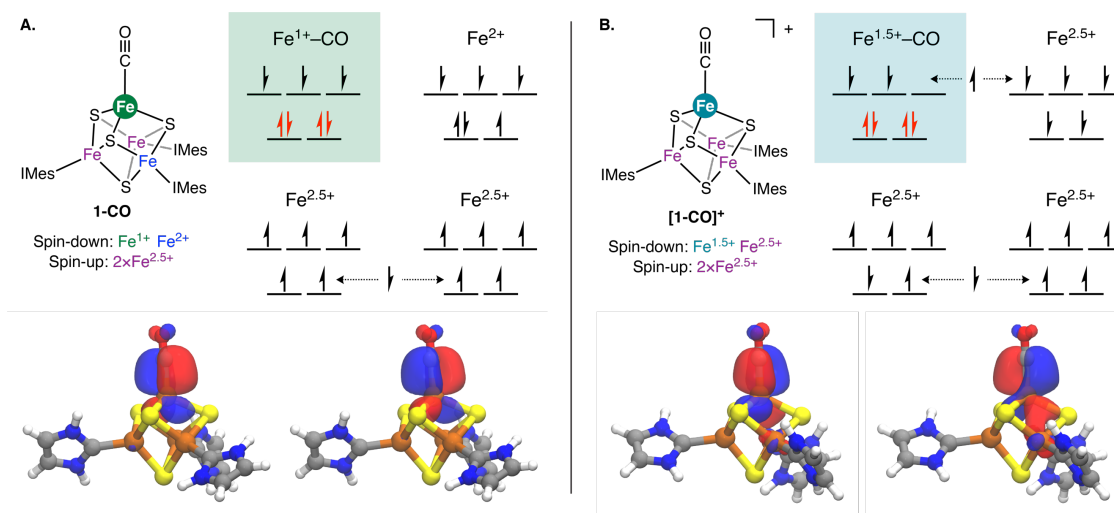


Figure 4. Qualitative calculated molecular orbital diagrams for **1-CO** (A) and **[1-CO]⁺** (B) showing the fully populated Fe–CO π-backbonding orbitals (highlighted in red). The isosurface plots (bottom, 0.04 au) show the localized π-backbonding orbitals in the α-spin manifold. See SI for computational details.

aligned NHC-ligated Fe center (Fig. 4B). Calculations using the TPSSh functional converge to an electronic structure more similar to that of **1-CO**, except one of the α-spin electrons involved in Fe–CO π-backbonding is further delocalized between the Fe–CO and the spin-aligned Fe–NHC center (see SI). We favor the electronic structure obtained using the TPSS functional because the [Fe₄S₄]⁺ core of an optimized structure displays pseudo-C_{3v} symmetry akin to that observed in the X-ray crystal structure of **[1-CO]⁺** (see SI). Regardless of the functional chosen, a Löwdin population analysis of the Fe-centered orbitals in **[1-CO]⁺** leads to approximate valence assignments as follows: Fe^{1.5+} for the Fe–CO, Fe^{2.5+} for the spin-aligned Fe–NHC site, and 2×Fe^{2.5+} for the remaining NHC ligated sites (see SI). The computed valence for the Fe–CO site in **[1-CO]⁺** is higher than that in **1-CO**, which is consistent with its weaker extent of C–O bond activation ($\Delta\nu(\text{C–O}) = 70 \text{ cm}^{-1}$) as well as its shorter Fe–S and longer Fe–CO bond lengths (Table 1).

The experimental and computational analysis presented above demonstrates that Fe–S clusters can achieve low-valent electronic configurations at individual Fe sites, allowing for substantial activation of π-accepting substrates such as CO. Such configurations are generated by an intracuster electron transfer process that is conceptually related to valence rearrangements observed in other metalloclusters^{24,60–63} in

which the existing metal ion valences are shuffled between cluster sites. However, the processes observed for **1-CO** and $[\mathbf{1-CO}]^+$ are distinct in that CO binding induces generation of valences that were not initially present in the cluster. To illustrate, consider the valence distributions possible for $[\text{Fe}_4\text{S}_4]^0$ clusters (the core charge state in **1-CO**): in the canonical, all-ferrous electronic structure, no valence rearrangement can occur because each Fe has the same valence (Fe^{2+}). Instead, we showed that CO binding induces valence disproportionation, which entails electron transfer from an NHC-ligated Fe center to the Fe–CO center, splitting two Fe^{2+} valences to generate $\text{Fe}^{1+}\text{-CO}$ and an Fe^{3+} center (the latter is additionally stabilized by generation of a mixed-valent $2\times\text{Fe}^{2.5+}\text{-NHC}$ pair). Low-valent configurations are likewise accessed in $[\mathbf{1-CO}]^+$ by partial disproportionation of $2\times\text{Fe}^{2+}$ centers to give a configuration with substantial $\text{Fe}^{1+}/\text{Fe}^{3+}$ character. In both cases, the formal oxidation of NHC-bound Fe sites is accompanied by substantial Fe–S bond contraction, indicating a role for the entire cluster in promoting C–O bond weakening.^{64,65}

The ability to undergo valence disproportionation allows for the generation of low-valent configurations without necessitating super-reduction of an Fe^{2+} site in an all-ferrous cluster to Fe^{1+} . For $[\text{Fe}_4\text{S}_4]$ clusters in particular, such super-reduced states (*i.e.*, $[\text{Fe}_4\text{S}_4]^{1-}$) have not been characterized and would presumably only be generated at extremely low potentials. However, two related questions remain regarding the biological relevance of the low-valent states we observe: (1) Do the synthetic clusters reported herein have access to low-valent configurations only because they are supported by NHC ligands (as opposed to biologically relevant donors such as thiolates); and (2) Would the redox states at which we observe low-valent configurations be accessible at physiologically relevant potentials?

To address the first question, we compare the redox properties of **2** and $[\mathbf{2}]^+$ with those of synthetic, thiolate-ligated $[\text{Fe}_4\text{S}_4]$ clusters. The $[\text{Fe}_4\text{S}_4]^+$ state in $[\text{Fe}_4\text{S}_4(\text{SPh})_4]^{3-}$ is stable between -2.13 and -1.40 V (vs. Fc/Fc^+ , in MeCN),⁴⁴ whereas the analogous state in $[\mathbf{2}]^+$ is stable in an anodically shifted window: between -1.91 V and -0.75 V (vs. Fc/Fc^+ , in *o*-DFB). This illustrates that NHC-ligated clusters are less reducing than their thiolate-ligated analogues,⁴⁶ and we therefore conclude that the intramolecular electron

transfer process that generates low-valent Fe in **1-CO** and **[1-CO]⁺** is not a result of the NHC-ligands rendering the cluster especially reducing. For this reason, we expect that if **1-CO** and **[1-CO]⁺** were supported by thiolates instead of IMes, we would similarly observe low-valent electronic configurations.

To address the second question, we first note that the redox state of **[1-CO]⁺** ($[\text{Fe}_4\text{S}_4]^+$) is commonly observed in biology,^{4,6} and, although rarer, that of **1-CO** ($[\text{Fe}_4\text{S}_4]^0$) has also been characterized in Fe-S proteins.⁶⁶⁻⁶⁹ However, direct comparisons between the potentials at which these states are generated in biological systems and synthetic systems cannot be made because of the different conditions in which the potentials were determined; this is well-established^{70,71} for thiolate-ligated clusters where the redox potentials of biological $[\text{Fe}_4\text{S}_4]$ clusters are shifted anodically relative to those of synthetic $[\text{Fe}_4\text{S}_4]$ clusters. Nevertheless, we can consider how CO binding would affect the redox couples of Fe-S clusters. Because of the strong π -acidity of CO, we would expect an anodic shift upon substituting an NHC or thiolate for CO. This is observed experimentally for the molecules described herein; for **[1-CO]⁺**, the $[\text{Fe}_4\text{S}_4]^{1+}$ state is stable between -1.54 and -0.50 V, compared with -1.91 to -0.75 V for **[2]⁺** (both vs. Fc/Fc⁺ under identical conditions; see SI). Likewise, CO binding to a thiolate-ligated, biological $[\text{Fe}_4\text{S}_4]$ cluster would anodically shift the cluster's redox couples, and therefore the redox states at which we observe low-valent Fe ($[\text{Fe}_4\text{S}_4]^0$ and $[\text{Fe}_4\text{S}_4]^+$) would remain accessible using biological reductants. On this basis, we surmise that low-valent Fe centers can be generated in Fe-S clusters at physiologically accessible redox potentials.

Conclusion

In conclusion, we have shown that Fe–S clusters, even when comprised of exclusively Fe²⁺ and Fe³⁺ ions, can undergo intramolecular valence disproportionation to access low-valent electronic configurations. This expands the range of characterized electronic configurations for formally mid-valent Fe–S clusters and connects the chemistry of Fe–S clusters to that of low-valent Fe. Moreover, these low-valent configurations enable substantial substrate bond activation without having to proceed through highly negative redox couples; this design principle can be further exploited in catalysis and may account for Nature's utilization of Fe–S clusters for activating some of the strongest bonds in the biosphere.

Acknowledgements

We thank Dr. Peter Müller for assistance with XRD experiments. This work was supported by the U.S. Department of Energy, Office of Science, Office of Basic Energy Sciences, Division of Chemical Sciences, Geosciences, and Biosciences under Award #DE-SC0020974 to D.L.M.S. Seed funding was provided by the American Chemical Society Petroleum Research Fund (60568-DNI3 to D.L.M.S.). A.C.B. acknowledges fellowships from the National Science Foundation (Graduate Research Fellowship #1122374) and the Fannie and John Hertz Foundation, and N.B.T. acknowledges a fellowship from the National Institute of General Medical Sciences of the National Institutes of Health under award #F32GM137478.

Competing interests

The authors declare no competing interests.

References

- (1) Beinert, H.; Sands, R. H. Studies on succinic and DNPH dehydrogenase preparations by Paramagnetic Resonance (EPR) Spectroscopy. *Biochem. Biophys. Res. Commun.* **1960**, *3* (1), 41–46.
- (2) Orme-Johnson, W. H. Iron-sulfur proteins: Structure and function. *Annu. Rev. Biochem.* **1973**, *42*, 159–204.
- (3) Flint, D. H.; Allen, R. M. Iron-sulfur proteins with nonredox functions. *Chem. Rev.* **1996**, *96* (7), 2315–2334.
- (4) Beinert, H.; Holm, R. H.; Münck; Eckard. Iron-sulfur clusters: Nature's modular, multipurpose structures. *Science* **1997**, *277* (5326), 653–659.
- (5) Hagen, W. R. EPR spectroscopy of iron–sulfur proteins. *Adv. Inorg. Chem.* **1992**, *38*, 165–222.
- (6) Beinert, H. Iron-sulfur proteins: Ancient structures, still full of surprises. *J. Biol. Inorg. Chem.*

2000, 5 (1), 2–15.

- 7) Beck, B. W. Highly-reduced metal carbonyls. **1991**, 30 (2), 168–169.
- (8) Sharma, V. K. Ferrate(VI) and Ferrate(V) oxidation of organic compounds: Kinetics and mechanism. *Coord. Chem. Rev.* **2013**, 257 (2), 495–510.
- (9) Berry, J. F.; Bill, E.; Bothe, E.; DeBeer George, S.; Meinert, B.; Neese, F.; Wieghardt, K. An octahedral coordination complex of iron(VI). *Science* **2006**, 312 (5782), 1937–1941.
- (10) Martinez, J. L.; Lutz, S. A.; Yang, H.; Xie, J.; Telsler, J.; Hoffman, B. M.; Carta, V.; Pink, M.; Losovyj, Y.; Smith, J. M. Structural and spectroscopic characterization of an Fe(VI) bis(imido) complex. *Science* **2020**, 370, 356–359.
- (11) Hagen, W. R. EPR spectroscopy of complex biological iron–sulfur systems. *J. Biol. Inorg. Chem.* **2018**, 23 (4), 623–634.
- (12) Gall, R. S., Chu, C. T. W. and Dahl, L. F. Preparation, structure, and bonding of two cubane-like iron-nitrosyl complexes, $\text{Fe}_4(\text{NO})_4(\mu_3\text{-S})_4$ and $\text{Fe}_4(\text{NO})_4(\mu_3\text{-S}_2)(\mu_3\text{-NC}(\text{CH}_3)_3)_2$: Stereochemical consequences of bridging ligand substitution on a completely bonding tetrametal cluster unit and of different terminal ligands on the cubane-like Fe_4S_4 core. *J. Am. Chem. Soc.* **1974**, 96 (12), 4019–4023.
- (13) Ting-Wah Chu, C., Yip-Kwai Lo, F. and Dahl, L. F. Synthesis and stereochemical analysis of the $[\text{Fe}_4(\text{NO})_4(\mu_3\text{-S})_4]^n$ Series ($n = 0, -1$) which possesses a cubanelike Fe_4S_4 core: direct evidence for the antibonding tetrametal character of the unpaired electron upon a one-electron reduction of a completely bonding tetrahedral metal cluster. *J. Am. Chem. Soc.* **1982**, 104 (12), 3409–3422.
- (14) Goh, C. and Holm, R. H. Synthesis and structures of the cuboidal iron-sulfur-nitrosyl-phosphine clusters $[\text{Fe}_4\text{S}_3(\text{NO})_4(\text{PR}_3)_3]^{0,1+}$ ($\text{R} = \text{Et}, \text{Pr}^i, \text{C}_6\text{H}_{11}$). *Inorg. Chim. Acta* **1998**, 270 (4), 46–54.
- (15) Hopmann, K. H., Ghosh, A. & Noodleman, L. Density functional theory calculations on Mössbauer parameters of nonheme iron nitrosyls. *Inorg. Chem.* **2009**, 48 (19), 9155–9165.
- (16) Rodriguez, M. M.; Stubbert, B. D.; Scarborough, C. C.; Brennessel, W. W.; Bill, E.; Holland, P.

- L. Isolation and characterization of stable iron(I) sulfide complexes. *Angew. Chem. Int. Ed.* **2012**, *51* (33), 8247–8250.
- (17) Anderson, J. S. and Peters, J. C. Low-spin pseudotetrahedral iron(I) sites in $\text{Fe}_2(\mu\text{-S})$ complexes. *Angew. Chem. Int. Ed.* **2014**, *53* (23), 5978–5981.
- (18) DeRoshia, D. E.; Chilkuri, V. G.; Van Stappen, C.; Bill, E.; Mercado, B. Q.; DeBeer, S.; Neese, F.; Holland, P. L. Planar three-coordinate iron sulfide in a synthetic $[\text{4Fe-3S}]$ cluster with biomimetic reactivity. *Nat. Chem.* **2019**, *11* (11), 1019–1025.
- (19) Ray, M.; Golombek, A. P.; Hendrich, M. P.; Young, V. G.; Borovik, A. S. Synthesis and structure of a trigonal monopyramidal Fe(II) complex and its paramagnetic carbon monoxide derivative. *J. Am. Chem. Soc.* **1996**, *118* (25), 6084–6085.
- (20) Nguyen, D. H.; Hsu, H. F.; Millar, M.; Koch, S. A.; Achim, C.; Bominaar, E. L.; Münck, E. Nickel(II) thiolate complex with carbon monoxide and its Fe(II) analog: Synthetic models for CO adducts of nickel-iron-containing enzymes. *J. Am. Chem. Soc.* **1996**, *118* (37), 8963–8964.
- (21) Davies, S. C.; Durrant, M. C.; Hughes, D. L.; Richards, R. L.; Roger Sanders, J. Iron, cobalt and vanadium complexes of the $\text{N}(\text{CH}_2\text{CH}_2\text{S})_3^{3-}$ ligand with chloride, azide, cyanide and carbonyl co-ligands. *J. Chem. Soc. Dalt. Trans.* **2000**, No. 24, 4694–4701.
- (22) Lee, Y.; Peters, J. C. Silylation of iron-bound carbon monoxide affords a terminal Fe carbyne. *J. Am. Chem. Soc.* **2011**, *133* (12), 4438–4446.
- (23) Rittle, J.; Peters, J. C. Fe- N_2/CO complexes that model a possible role for the interstitial C atom of FeMo-cofactor (FeMoco). *Proc. Natl. Acad. Sci. U.S.A.* **2013**, *110* (40), 15898–15903.
- (24) Arnett, C. H.; Chalkley, M. J.; Agapie, T. A Thermodynamic model for redox-dependent binding of carbon monoxide at site-differentiated, high spin iron clusters. *J. Am. Chem. Soc.* **2018**, *140* (16), 5569–5578.
- (25) Bloch, E. D.; Hudson, M. R.; Mason, J. A.; Chavan, S.; Crocellà, V.; Howe, J. D.; Lee, K.; Dzubak, A. L.; Queen, W. L.; Zadrozny, J. M.; Geier, S. J.; Lin, L. C.; Gagliardi, L.; Smit, B.;

- Neaton, J. B.; Bordiga, S.; Brown, C. M.; Long, J. R. Reversible CO binding enables tunable CO/H₂ and CO/N₂ separations in metal-organic frameworks with exposed divalent metal cations. *J. Am. Chem. Soc.* **2014**, *136* (30), 10752–10761.
- (26) Lee, C. C.; Hu, Y.; Ribbe, M. W. Vanadium nitrogenase reduces CO. *Science* **2010**, *329* (5992), 642.
- (27) Hu, Y.; Lee, C. C.; Ribbe, M. W. Extending the carbon chain: Hydrocarbon formation catalyzed by vanadium/molybdenum nitrogenases. *Science* **2011**, *333* (6043), 753–755.
- (28) Yang, Z. Y.; Dean, D. R.; Seefeldt, L. C. Molybdenum nitrogenase catalyzes the reduction and coupling of CO to form hydrocarbons. *J. Biol. Chem.* **2011**, *286* (22), 19417–19421.
- (29) Seefeldt, L. C.; Yang, Z. Y.; Lukoyanov, D. A.; Harris, D. F.; Dean, D. R.; Raugei, S.; Hoffman, B. M. Reduction of substrates by nitrogenases. *Chem. Rev.* **2020**, *120* (12), 5082–5106.
- (30) Lee, C. C.; Hu, Y.; Ribbe, M. W. ATP-independent formation of hydrocarbons catalyzed by isolated nitrogenase cofactors. *Angew. Chem. Int. Ed.* **2012**, *51* (8), 1947–1949.
- (31) Lee, C. C.; Hu, Y.; Ribbe, M. W. Catalytic reduction of CN⁻, CO, and CO₂ by nitrogenase cofactors in lanthanide-driven reactions. *Angew. Chem. Int. Ed.* **2015**, *54* (4), 1219–1222.
- (32) Lee, C. C.; Hu, Y.; Ribbe, M. W. Insights into hydrocarbon formation by nitrogenase cofactor homologs. *MBio* **2015**, *6* (2), 1–6.
- (33) Tanifuji, K.; Lee, C. C.; Ohki, Y.; Tatsumi, K.; Hu, Y.; Ribbe, M. W. Combining a nitrogenase scaffold and a synthetic compound into an artificial enzyme. *Angew. Chem. Int. Ed.* **2015**, *54* (47), 14022–14025.
- (34) Sickerman, N. S.; Tanifuji, K.; Lee, C. C.; Ohki, Y.; Tatsumi, K.; Ribbe, M. W.; Hu, Y. Reduction of C1 substrates to hydrocarbons by the homometallic precursor and synthetic mimic of the nitrogenase cofactor. *J. Am. Chem. Soc.* **2017**, *139* (2), 603–606.
- (35) Stiebritz, M. T.; Hiller, C. J.; Sickerman, N. S.; Lee, C. C.; Tanifuji, K.; Ohki, Y.; Hu, Y. Ambient conversion of CO₂ to hydrocarbons by biogenic and synthetic [Fe₄S₄] clusters. *Nat.*

Catal. **2018**, *1* (6), 444–451.

- (36) Lee, C. C.; Tanifuji, K.; Newcomb, M.; Liedtke, J.; Hu, Y.; Ribbe, M. W. A comparative analysis of the CO-reducing activities of MoFe Proteins containing Mo- and V-Nitrogenase cofactors. *ChemBioChem* **2018**, *19* (7), 649–653.
- (37) Brown, A. C.; Suess, D. L. M. Controlling Substrate Binding to Fe₄S₄ Clusters through Remote Steric Effects. *Inorg. Chem.* **2019**, *58* (8), 5273–5280.
- (38) Han, J.; Coucouvanis, D. A new function of the (μ₃-S) ligand in an Fe₄S₄ cluster: synthesis and structure of the high-nuclearity Mo/Fe/S Cluster, Fe(DMF)Cl(Cl₄-cat)₂-Mo₂Fe₂S₄(PEt₃)₂ClFe₄S₄(PEt₃)₃ (CO)₆Cl. *J. Am. Chem. Soc.* **2002**, *123* (45), 11304–11305.
- (39) Ogino, H.; Inomata, S.; Tobita, H. Abiological iron–sulfur clusters. *Chem Rev.* **1998**, *98*, 2093–2121.
- (40) Spatzal, T.; Perez, K. A.; Einsle, O.; Howard, J. B.; Rees, D. C. Ligand binding to the FeMo-cofactor: Structures of CO-bound and reactivated nitrogenase. *Science* **2014**, *345* (6204), 1620–1623.
- (41) Rohde, M.; Grunau, K.; Einsle, O. CO binding to the FeV cofactor of CO-reducing vanadium nitrogenase at atomic resolution. *Angew. Chem. Int. Ed.* **2020**, *59* (52), 23626–23630.
- (42) Buscagan, T. M.; Perez, K. A.; Maggiolo, A. O.; Rees, D. C.; Spatzal, T. Structural characterization of two CO molecules bound to the nitrogenase active site. *Angew. Chem. Int. Ed.* **2021**, *60* (11), 5704–5707
- (43) Peters, J. C.; Johnson, A. R.; Odom, A. L.; Wanandi, P. W.; Davis, W. M.; Cummins, C. C. Assembly of molybdenum/titanium μ-oxo complexes via radical alkoxide C-O cleavage. *J. Am. Chem. Soc.* **1996**, *118* (42), 10175–10188.
- (44) Zhou, C.; Raebiger, J. W.; Segal, B. M.; Holm, R. H. The influence of net charge on the redox potentials of Fe₄S₄ cubane-type clusters in aprotic solvents. *Inorganica Chim. Acta* **2000**, *300*–*302*, 892–902.

- (45) Scott, T. A.; Berlinguette, C. P.; Holm, R. H.; Zhou, H.-C. Initial synthesis and structure of an all-ferrous analogue of the fully reduced $[\text{Fe}_4\text{S}_4]^0$ cluster of the nitrogenase iron protein. *Proc. Natl. Acad. Sci. U.S.A.* **2005**, *102* (28), 9741–9744.
- (46) Deng, L.; Holm, R. H. Stabilization of fully reduced iron-sulfur clusters by carbene ligation: The $[\text{Fe}_n\text{S}_n]^0$ oxidation levels ($n = 4, 8$). *J. Am. Chem. Soc.* **2008**, *130* (30), 9878–9886.
- (47) Kisko, J. L.; Hascall, T.; Parkin, G. The synthesis, structure, and reactivity of phenyl tris(3-tert-butylpyrazolyl)borato iron methyl, $[\text{PhTp}(\text{Bu}^t)]\text{FeMe}$: Isolation of a four-coordinate monovalent iron carbonyl complex, $[\text{PhTp}(\text{Bu}^t)]\text{FeCO}$. *J. Am. Chem. Soc.* **1998**, *120* (40), 10561–10562.
- (48) Yang, L.; Powell, D. R.; Houser, R. P. Structural variation in copper(I) complexes with pyridylmethylamide ligands: Structural analysis with a new four-coordinate geometry index, τ_4 . *J. Chem. Soc. Dalton Trans.* **2007**, No. 9, 955–964.
- (49) Hawrelak, E. J.; Bernskoetter, W. H.; Lobkovsky, E.; Yee, G. T.; Bill, E.; Chirik, P. J. Square planar vs tetrahedral geometry in four coordinate iron(II) complexes. *Inorg. Chem.* **2005**, *44* (9), 3103–3111.
- (50) Milocco, F.; De Vries, F.; Siebe, H. S.; Engbers, S.; Demeshko, S.; Meyer, F.; Otten, E. Widening the window of spin-crossover temperatures in bis(formazanate)iron(II) complexes via steric and noncovalent interactions. *Inorg. Chem.* **2021**, *60* (3), 2045–2055.
- (51) Liu, Y.; Luo, L.; Xiao, J.; Wang, L.; Song, Y.; Qu, J.; Luo, Y.; Deng, L. Four-coordinate iron(II) diaryl compounds with monodentate N-Heterocyclic carbene ligation: Synthesis, characterization, and their tetrahedral-square planar isomerization in solution. *Inorg. Chem.* **2015**, *54* (10), 4752–4760.
- (52) Venkateswara Rao, P.; Holm, R. H. Synthetic analogues of the active sites of iron-sulfur proteins. *Chem. Rev.* **2004**, *104* (2), 527–560.
- (53) Pandelia, M. E.; Lanz, N. D.; Booker, S. J.; Krebs, C. Mössbauer spectroscopy of Fe/S proteins. *Biochim. Biophys. Acta - Mol. Cell Res.* **2015**, *1853* (6), 1395–1405.

- (54) Ye, S.; Bill, E.; Neese, F. Electronic structures of the $[\text{Fe}(\text{N}_2)(\text{SiP}^i\text{Pr}_3)]^{+1/0/-1}$ electron transfer series: A counterintuitive correlation between isomer shifts and oxidation states. *Inorg. Chem.* **2016**, *55* (7), 3468–3474.
- (55) Chakrabarti, M.; Deng, L.; Holm, R. H.; Münck, E.; Bominaar, E. L. Mössbauer, electron paramagnetic resonance, and theoretical studies of a carbene-based all-ferrous Fe_4S_4 cluster: Electronic origin and structural identification of the unique spectroscopic site. *Inorg. Chem.* **2009**, *48* (7), 2735–2747.
- (56) Spiller, N.; Bjornsson, R.; Debeer, S.; Neese, F. Carbon monoxide binding to the iron-molybdenum cofactor of nitrogenase: A detailed quantum mechanics/molecular mechanics investigation. *Inorg. Chem.* **2021**, *60* (23), 18031–18047.
- (57) Noodleman, L.; Peng, C. Y.; Case, D. A.; Mouesca, J. M. Orbital interactions, electron delocalization and spin coupling in iron-sulfur clusters. *Coord. Chem. Rev.* **1995**, *144* (C), 199–244.
- (58) Monesca, J. M.; Chen, J. L.; Noodleman, L.; Bashford, D.; Case, D. A. Density Functional/Poisson-Boltzmann calculations of redox potentials for iron-sulfur clusters. *J. Am. Chem. Soc.* **1994**, *116* (26), 11898–11914.
- (59) Bjornsson, R.; Lima, F. A.; Spatzal, T.; Weyhermüller, T.; Glatzel, P.; Bill, E.; Einsle, O.; Neese, F.; DeBeer, S.; Hoffman, B. M. Identification of a spin-coupled Mo(III) in the nitrogenase iron-molybdenum cofactor. *Chem. Sci.* **2014**, *5* (8), 3096–3103.
- (60) Pantazis, D. A.; Ames, W.; Cox, N.; Lubitz, W.; Neese, F. Two interconvertible structures that explain the spectroscopic properties of the oxygen-evolving complex of photosystem II in the S2 state. *Angew. Chem. Int. Ed.* **2012**, *51* (39), 9935–9940.
- (61) Kuppuswamy, S.; Powers, T. M.; Johnson, B. M.; Brozek, C. K.; Krogman, J. P.; Bezpalko, M. W.; Berben, L. A.; Keith, J. M.; Foxman, B. M.; Thomas, C. M. One-electron oxidation chemistry and subsequent reactivity of diiron imido complexes. *Inorg. Chem.* **2014**, *53* (11), 5429–5437.

- (62) Eames, E. V.; Betley, T. A. Site-isolated redox reactivity in a trinuclear iron complex. *Inorg. Chem.* **2012**, *51* (19), 10274–10278.
- (63) Anderton, K. J.; Knight, B. J.; Rheingold, A. L.; Abboud, K. A.; García-Serres, R.; Murray, L. J. Reactivity of hydride bridges in a high-spin $[\text{Fe}_3(\mu\text{-H})_3]^{3+}$ cluster: Reversible H_2/CO exchange and Fe-H/B-F bond metathesis. *Chem. Sci.* **2017**, *8* (5), 4123–4129.
- (64) Powers, T. M.; Betley, T. A. Testing the polynuclear hypothesis: Multielectron reduction of small molecules by triiron reaction sites. *J. Am. Chem. Soc.* **2013**, *135* (33), 12289–12296.
- (65) McSkimming, A.; Suess, D. L. M. Dinitrogen binding and activation at a molybdenum–iron–sulfur cluster. *Nat. Chem.* **2021**, *13* (7), 666–670..
- (66) Angove, H. C.; Yoo, S. J.; Burgess, B. K.; Münck, E. Mössbauer and EPR evidence for an all-ferrous Fe_4S_4 cluster with $S = 4$ in the Fe protein of nitrogenase. *J. Am. Chem. Soc.* **1997**, *119* (37), 8730–8731.
- (67) Yoo, S. J.; Angove, H. C.; Burgess, B. K.; Hendrich, M. P.; Münck, E. Mossbauer and integer-spin EPR studies and spin-coupling analysis of the $[\text{4Fe-4S}]^0$ cluster of the Fe protein from *Azotobacter vinelandii* nitrogenase. *J. Am. Chem. Soc.* **1999**, *121* (11), 2534–2545.
- (68) Hans, M.; Buckel, W.; Bill, E. Spectroscopic evidence for an all-ferrous $[\text{4Fe-4S}]^0$ cluster in the superreduced activator of 2-hydroxyglutaryl-CoA dehydratase from *Acidaminococcus fermentans*. *J. Biol. Inorg. Chem.* **2008**, *13* (4), 563–574.
- (69) Lowery, T. J.; Wilson, P. E.; Zhang, B.; Bunker, J.; Harrison, R. G.; Nyborg, A. C.; Thiriot, D.; Watt, G. D. Flavodoxin hydroquinone reduces *Azotobacter vinelandii* Fe protein to the all-ferrous redox state with a $S = 0$ spin state. *Proc. Natl. Acad. Sci. U.S.A.* **2006**, *103* (46), 17131–17136.
- (70) Hill, C. L.; Renaud, J.; Holm, R. H.; Mortenson, L. E. Synthetic analogues of the active sites of iron-sulfur proteins. 15. Comparative polarographic potentials of the $[\text{Fe}_4\text{S}_4(\text{SR})_4]^{2-,3-}$ and *Clostridium pasteurianum* ferredoxin redox couples. *J. Am. Chem. Soc.* **1977**, *99* (8), 2549–2557.
- (71) Watt, G. D.; Reddy, K. R. N. Formation of an all ferrous $[\text{Fe}_4\text{S}_4]$ cluster in the iron protein

component of *Azotobacter vinelandii* nitrogenase. *J. Inorg. Biochem.* **1994**, 53 (4), 281–294.

TOC graphic:

